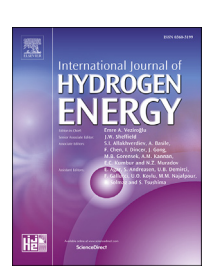


Available online at www.sciencedirect.com

ScienceDirect

journal homepage: www.elsevier.com/locate/he



Review Article

Improved direct field oriented control of multiphase induction motor used in hybrid electric vehicle application



Koussaila Iffouzar ^{a,*}, Bessam Amrouche ^b, Tahar Otmane Cherif ^b, Mohamed-Fouad Benkhoris ^c, Djamal Aouzellag ^a, Kaci Ghedamsi ^a

ARTICLE INFO

Article history:
Received 26 March 2017
Received in revised form
23 June 2017
Accepted 23 June 2017
Available online 13 July 2017

Keywords:
Hybrid electric vehicle
Fuel cell
Ultra-capacitor
Multiphase electrical drive
Torque ripples

ABSTRACT

This paper presents an improved direct rotor field oriented control of seven phase induction motor in hybrid electric vehicle (HEV) system. The dynamic model of the machine shows that non-sequential currents producing no torque appear and degrade the quality of currents. Further, the fuzzy logic controller is proposed to filter non-sequential components and improves the quality energy. Hybridization of the electric vehicle by a fuel cell (HEV) and an auxiliary energy source has the advantage of improving the dynamic response and efficiency of the system. Indeed, an ultra-capacitor (UC) used as a means of energy storage to enable the lower dynamic FC when changes in power fast and recovers braking energy as well as absorption of immanent disturbances of the static converters. Improving the quality of energy demand can improve not only the lifetime of the actuator but also the onboard sources. One of the results of the reduction of interference in the system induces to the reduction of mechanical vibrations, which generates quieter systems, which is an advantage for these urban transport applications. In this paper, the modeling of the different parts of the multi-physical system that represent hybrid vehicle are presented. The performance of the aimed system is analysed under different acting conditions.

© 2017 Hydrogen Energy Publications LLC. Published by Elsevier Ltd. All rights reserved.

Contents

Introduction	19297
System description	19297
System modeling	19298

^a Laboratoire de Maitrise des Energies Renouvelables, Faculté de Technologie, Université de Bejaia 06000, Algeria

^b Laboratoire de Conception et Conduite des Systèmes de Production (L2CSP), Faculté de Génie Electrique et Informatique, Université de Tizi Ouzou 15000, Algeria

^c Institut de Recherche en Energie Electrique de Nantes Atlantique, Polytech de Nantes, France

^{*} Corresponding author.

Dynamic modeling of seven phase induction motor	19298
PEMFC dynamics model	19300
UC system modeling	19301
Dynamics model of vehicle	
Electrical differential	19301
Control system	. 19302
Direct field oriented control of seven phase induction motor	19302
DC bus voltage regulation and UC converter control	19304
Fc converters control	19304
Simulation results and interpretation	. 19304
Conclusion	. 19308
References	. 19308

Introduction

For over a century, electric machines have played a leading role in industrial applications because of the flexibility of their implementation and the importance of the applications in which they can be integrated. Since the end of the Second World War, the use of electric machines has been stimulated by an increase in the demand for consumer goods requiring more efficient means of industrial production in order to best respond to this increase. It is found everywhere and in the most trivial distraction systems for the consumer-buyer, to the most advanced applications attached, for example, health, production, control, energy, transport and space exploration. The current reality does not deny the increased use of electric machines. The individual and collective awareness of the limitation of fossil resources and the need to limit polluting emissions calls into question the actuators based on thermodynamic laws. A new era is to replace as much as possible electric actuators to certainly too polluting machines.

Since 40 years, thanks to the development of power electronics and fast microprocessors many researches have carried on the area of vector control of conventional AC machines [1]. Various vector control techniques are investigated as rotor-flux-oriented control, stator-flux-oriented control, and magnetizing-flux-oriented control [2,3]. Several control techniques are elaborated with/without position sensors, associated with several techniques of physical quantities estimation. In high power range, the segmentati SOx on of this late is required. An alternative consists to investigate a novel electrical drive family, constituted by high number of phases [4–9]. By increasing the number of phases, it is also possible increasing the torque per ampere for the same machine volume. But, the application of these decoupled control is not sufficient in the case of a multiphase induction machine, the quality of energy conveyed inside the machine is deteriorated by non-sequential currents engendered by voltage harmonics.

A new control of the seven-phase induction machine with minimization of the non-sequential currents using the fuzzy logic contrary to the solutions proposed in Ref. [10] which consists in the installation of a filter in series with the winding of the motor which is bulky And which is not adapted to this type of application, since the filtering is carried out in a permanent regime.

Safeguarding the environment has led humankind in recent years to reduce emissions of greenhouse gases. This pollution originates mainly from incomplete combustion and especially from thermal vehicles. To help improve air quality, the electric vehicle (EV) is a good initiative for safeguarding the environment.

The emissions related to vehicle propulsion (CO2, SOx and NO_x) have a significant responsibility for environmental problems such as the greenhouse effect, acid rain and air pollution. It is reported that the CO₂ emissions from vehicle accounts for about 30%-55% of total CO2 emissions in the world. Some solutions have been realized in the past few years for vehicle applications with fuel cell (FC) [11-17], for this a dynamic model of the fuel cell was developed during this work. However, the Fuel cell cannot meet the power transition which need a second energy source such as ultra capacitor. The control of the UC converter allows the regulation of the DC bus voltage. The vehicle speed is adjusted by the inverters controls. For the FC converter, an algorithm is implemented to control the reference power. Several simulations results using Matlab/Simulink will be presented. The improvement of the quality of the energy of the training system leads to the improvement of the quality of the power to demand and thus the life of the elements of the source embark on this lengthening. The impact of such a system is indisputable in naval applications and electric propulsion.

This paper will be organized into four main sections; the first part will be the modeling of the different elements of the system. The second part will deal with the control of the hybrid vehicle. In the third part, we will regain control of each element of the system. This work will close by the interpretation of the results as well as the resulting conclusion.

System description

The HEV is propelled by two seven-phase induction motor; each one is connected to the wheel. The global scheme of the HEV and power system of the FC/Uc is represented in Fig. 1. The two energy sources (FC and UC) exchange power with a

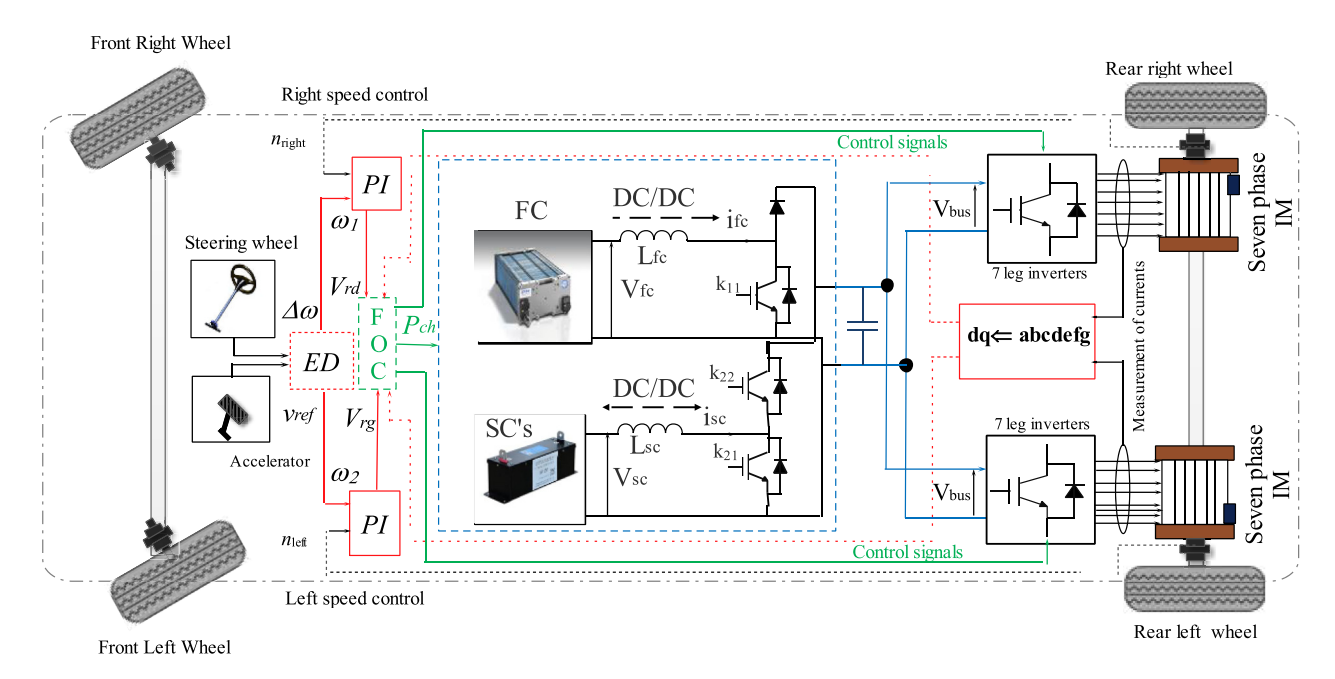


Fig. 1 - Global scheme of HEV system.

DC bus. For the FC, a boost converter unidirectional in current is utilized to connect the FC to the DC bus; although, the UC requires DC/DC converter bidirectional in current to supply power and to recover the breaking energy. The two inductances added as filters and to respect sources alternation. The DC bus which is a capacitor supplies the both traction machines with employing a three levels seven phase inverter for each one to convert the DC power into AC power. This system gives the torque control of each wheel in dependently with a significantly high accuracy, which can enhance the stability of the HEV, reduce clutter caused by the mechanical part such as electrical differential and transmission shafts and give more frees space in the vehicle for UC and hydrogen tank. The seven phase induction machine type which is used in the transportation field due to its good power, high efficiency, weight ratio machines and it can still continue to run using the remaining phases without any external intervention in faults open phases [10-13].

System modeling

The modeling of each element constituting the multi-physical system, such as propulsion, energy sources and static converters are given in this section.

Dynamic modeling of seven phase induction motor

The winding axes of seven-stator winding are displaced by $2\pi/7$, generally inductance matrices of polyphase machines are

full, which means for controlling in a strongly coupled system. However, like all the stator inductance matrices (or rotor) are circulating, so they are diagonalizable. Hence there exists a unique orthogonal basis of eigenvectors on which the magnetic quantities of the machine are decoupled [8]. Assuming linear magnetic circuits, equal mutual inductances and neglecting iron losses, voltage equations of stator and rotor in the real frame are given by:

$$\begin{cases}
[v_s] = [R_s][i_s] + [L_s] \frac{d}{dt}[i_s] + \frac{d}{dt}[M_{sr}][i_r] \\
[v_r] = [R_r][i_r] + [L_r] \frac{d}{dt}[i_r] + \frac{d}{dt}[M_{rs}][i_s]
\end{cases}$$
(1)

$$[L_s] = \begin{bmatrix} l_s & m_{s1} & m_{s2} & m_{s3} & m_{s4} & m_{s5} & m_{s6} \\ m_{s6} & l_s & m_{s1} & m_{s2} & m_{s3} & m_{s4} & m_{s5} \\ m_{s5} & m_{s6} & l_s & m_{s1} & m_{s2} & m_{s3} & m_{s4} \\ m_{s4} & m_{s5} & m_{s6} & l_s & m_{s1} & m_{s2} & m_{s3} \\ m_{s3} & m_{s4} & m_{s5} & m_{s6} & l_s & m_{s1} & m_{s2} \\ m_{s2} & m_{s3} & m_{s4} & m_{s5} & m_{s6} & l_s & m_{s1} \\ m_{s1} & m_{s2} & m_{s3} & m_{s4} & m_{s5} & m_{s6} & l_s \\ \end{bmatrix}$$

$$m_{si} = m_s cos \left(i\frac{2\pi}{7}\right) \text{ and } l_s = l_{fs} + m_s$$

$$[L_r] = \begin{bmatrix} l_r & m_{r1} & m_{r2} & m_{r3} & m_{r4} & m_{r5} & m_{r6} \\ m_{r6} & l_r & m_{r1} & m_{r2} & m_{r3} & m_{r4} & m_{r5} \\ m_{r5} & m_{r6} & l_r & m_{r1} & m_{r2} & m_{r3} & m_{r4} \\ m_{r4} & m_{r5} & m_{r6} & l_r & m_{r1} & m_{r2} \\ m_{r3} & m_{r4} & m_{r5} & m_{r6} & l_r & m_{r1} \\ m_{r2} & m_{r3} & m_{r4} & m_{r5} & m_{r6} & l_r & m_{r1} \\ m_{r1} & m_{r2} & m_{r3} & m_{r4} & m_{r5} & m_{r6} & l_r \\ m_{r1} & m_{r2} & m_{r3} & m_{r4} & m_{r5} & m_{r6} & l_r \\ m_{r1} & m_{r2} & m_{r3} & m_{r4} & m_{r5} & m_{r6} & l_r \\ m_{r1} & m_{r2} & m_{r3} & m_{r4} & m_{r5} & m_{r6} & l_r \\ m_{r1} & m_{r2} & m_{r3} & m_{r4} & m_{r5} & m_{r6} & l_r \\ m_{r1} & m_{r2} & m_{r3} & m_{r4} & m_{r5} & m_{r6} & l_r \\ m_{r1} & m_{r2} & m_{r3} & m_{r4} & m_{r5} & m_{r6} & l_r \\ m_{r1} & m_{r2} & m_{r3} & m_{r4} & m_{r5} & m_{r6} & l_r \\ m_{r1} & m_{r2} & m_{r3} & m_{r4} & m_{r5} & m_{r6} & l_r \\ m_{r1} & m_{r2} & m_{r3} & m_{r4} & m_{r5} & m_{r6} \\ m_{r1} & l_{r} & l_{r} & l_{r} & l_{r} \\ m_{r2} & l_{r} & l_{r} & l_{r} & l_{r} \\ m_{r3} & l_{r} & l_{r} & l_{r} & l_{r} \\ m_{r4} & l_{r} & l_{r} & l_{r} & l_{r} \\ m_{r5} & l_{r} & l_{r} & l_{r} \\ m_{r6} & l_{r} & l_{r} & l_{r} \\ m_{r7} & l_{r} & l_{r} & l_{r} \\ m_{r8} & l$$

$$[M_{sr}] = \begin{bmatrix} m_1 & m_2 & m_3 & m_4 & m_5 & m_6 & m_7 \\ m_7 & m_1 & m_2 & m_3 & m_4 & m_5 & m_6 \\ m_6 & m_7 & m_1 & m_2 & m_3 & m_4 & m_5 \\ m_5 & m_6 & m_7 & m_1 & m_2 & m_3 & m_4 \\ m_4 & m_5 & m_6 & m_7 & m_1 & m_2 & m_3 \\ m_3 & m_4 & m_5 & m_6 & m_7 & m_1 & m_2 \\ m_2 & m_3 & m_4 & m_5 & m_6 & m_7 & m_1 \end{bmatrix}$$

$$\begin{aligned} m_r &= m_{sr} cos \left(\theta - (k-1) \frac{2\pi}{7}\right) \text{ with: } k=1,\ldots,6 \\ \text{And } \left[M_{sr}\right] &= \left[M_{rs}\right]^t \end{aligned}$$

Due to the difficulty of solving the system in the real base, we will move to the orthogonal basis $(\alpha, \beta, x_1, y_1, x_2, y_2)$ using the transformation T_7 .

$$T_7 = \sqrt{rac{2}{7}} egin{bmatrix} 1 & a_1 & a_2 & a_3 & a_4 & a_5 & a_6 \ 0 & b_1 & b_2 & b_3 & b_4 & b_5 & b_6 \ 1 & a_2 & a_4 & a_6 & a_8 & a_{10} & a_{12} \ 0 & b_2 & b_4 & b_6 & b_8 & b_{10} & b_{12} \ 1 & a_3 & a_6 & a_9 & a_{12} & a_{15} & a_{18} \ 0 & b_3 & b_6 & b_9 & b_{12} & b_{15} & b_{18} \ c & c & c & c & c & c & c \end{pmatrix}$$

with: $a_h = \cos(2h\pi/7)$, $b_h = \sin(2h\pi/7)$ and c = 1/2.

Applying this transformation to system (1) and after calculation and simplification, the voltage equation in the orthogonal basis are obtained:

System of Eq. (2) expresses the modeling of seven-phase induction machine, which is composed by three parts. In fact, the $(\alpha\beta)$ part is the principal and only submachine providing the torque. The two parts ((x1,y1),(x2,y2)) express the machine's losses; they do not contribute to the torque production. This model not practical for the development of a command because of the reference immobility, this is why the proposed model is moved to the (d,q,x_1,y_1,x_2,y_2) using $T_{76}=P(\theta)$. T_7 . The voltage equations of the seven phase induction motor are rewritten as follows:

$$\begin{cases}
v_{ds} = r_s i_{ds} - \omega_s \psi_{qs} + \frac{d}{dt} \psi_{ds} \\
v_{qs} = r_s i_{qs} + \omega_s \psi_{ds} + \frac{d}{dt} \psi_{qs} \\
v_{x1s} = r_s i_{x1s} + \frac{d}{dt} \psi_{x1s} \\
v_{y1s} = r_s i_{y1s} + \frac{d}{dt} \psi_{y1s} \\
v_{x2s} = r_s i_{x2s} + \frac{d}{dt} \psi_{x2s} \\
v_{y2s} = r_s i_{y2s} + \frac{d}{dt} \psi_{y2s} \\
0 = r_r i_{dr} + \frac{d}{dt} \psi_{dr} - \omega_r \psi_{dr} \\
0 = r_r i_{dr} + \frac{d}{dt} \psi_{qr} + \omega_r \psi_{dr}
\end{cases}$$
(3)

$$\begin{cases}
\begin{bmatrix} \left[\mathbf{u}_{s(\alpha\beta)} \right] \\ \left[\mathbf{u}_{s(\mathbf{x}1\mathbf{y}1)} \right] \\ \left[\mathbf{u}_{s(\mathbf{x}1\mathbf{y}1)} \right] \end{bmatrix} = \mathbf{r}_{s} \begin{bmatrix} \left[\mathbf{i}_{s(\alpha\beta)} \right] \\ \left[\mathbf{i}_{s(\mathbf{x}1\mathbf{y}1)} \right] \\ \left[\mathbf{i}_{s(\mathbf{x}1\mathbf{y}1)} \right] \end{bmatrix} + \left[\mathbf{L}_{s\alpha} \right] \frac{\mathbf{d}}{\mathbf{dt}} \begin{bmatrix} \left[\mathbf{i}_{s(\alpha\beta)} \right] \\ \left[\mathbf{i}_{s(\mathbf{x}1\mathbf{y}1)} \right] \\ \left[\mathbf{i}_{s(\mathbf{x}2\mathbf{y}1)} \right] \end{bmatrix} + \left[\mathbf{L}_{s\alpha} \right] \frac{\mathbf{d}}{\mathbf{dt}} \begin{bmatrix} \left[\mathbf{i}_{s(\alpha\beta)} \right] \\ \left[\mathbf{i}_{s(\mathbf{x}2\mathbf{y}2)} \right] \end{bmatrix} \\ \left[\left[\mathbf{i}_{r(\mathbf{x}1\mathbf{y}1)} \right] \\ \left[\mathbf{v}_{r(\mathbf{x}1\mathbf{y}1)} \right] \end{bmatrix} = \mathbf{r}_{r} \begin{bmatrix} \left[\mathbf{i}_{r(\alpha\beta)} \right] \\ \left[\mathbf{i}_{r(\mathbf{x}1\mathbf{y}1)} \right] \\ \left[\mathbf{i}_{r(\mathbf{x}1\mathbf{y}1)} \right] \end{bmatrix} + \left[\mathbf{L}_{r\alpha} \right] \frac{\mathbf{d}}{\mathbf{dt}} \begin{bmatrix} \left[\mathbf{i}_{r(\alpha\beta)} \right] \\ \left[\mathbf{i}_{r(\mathbf{x}1\mathbf{y}1)} \right] \\ \left[\mathbf{i}_{r(\mathbf{x}1\mathbf{y}1)} \right] \end{bmatrix} \\ + \frac{2}{7} \left[\mathbf{p}(\theta) \right] \frac{\mathbf{d}}{\mathbf{dt}} \begin{bmatrix} \left[\mathbf{i}_{s(\alpha\beta)} \right] \\ \left[\mathbf{i}_{s(\alpha\beta)} \right] \\ \left[\mathbf{i}_{s(\mathbf{x}1\mathbf{y}1)} \right] \\ \left[\mathbf{i}_{s(\mathbf{x}2\mathbf{y}1)} \right] \end{bmatrix}
\end{cases} \tag{2}$$

One advantage of the T_7 transformation is diagonalization inductance matrix, replacing (g with s) we get the matrix stator inductance, and replacing (g with r) we get the matrix rotor inductance.

$$p(\theta) = \begin{bmatrix} \cos(\theta) & -\sin(\theta) & 0 & 0 & 0 & 0 & 0 \\ \sin(\theta) & \cos(\theta) & 0 & 0 & 0 & 0 & 0 \\ 0 & 0 & 1 & 0 & 0 & 0 & 0 \\ 0 & 0 & 0 & 1 & 0 & 0 & 0 \\ 0 & 0 & 0 & 0 & 1 & 0 & 0 \\ 0 & 0 & 0 & 0 & 0 & 1 & 0 \\ 0 & 0 & 0 & 0 & 0 & 0 & 1 \end{bmatrix}$$

where the flux equations are given by:

$$\begin{cases} \psi_{ds} = (l_{fs} + L_m)i_{ds} + L_mi_{dr} \\ \psi_{qs} = (l_{fs} + L_m)i_{qs} + L_mi_{qr} \\ \psi_{x_{1s}} = l_{fs}i_{x_{1s}} \\ \psi_{y_{1s}} = l_{fs}i_{y_{1s}} \\ \psi_{x_{2s}} = l_{fs}i_{x_{2s}} \\ \psi_{y_{2s}} = l_{fs}i_{y_{2s}} \\ \psi_{dr} = (l_{fr} + L_m)i_{dr} + L_mi_{ds} \\ \psi_{qr} = (l_{fr} + L_m)i_{qr} + L_mi_{qs} \end{cases}$$

$$(4)$$

Substituting the equations of flux in the equations of voltages:

$$\begin{cases} v_{ds} = r_s i_{ds} - \omega_s \left[(l_{fs} + L_m) i_{qs} + L_m i_{qr} \right] + \frac{d}{dt} \left[(l_{fs} + L_m) i_{ds} + L_m i_{dr} \right] \\ v_{qs} = r_s i_{qs} + \omega_s \left[(l_{fs} + L_m) i_{ds} + L_m i_{dr} \right] + \frac{d}{dt} \left[(l_{fs} + L_m) i_{qs} + L_m i_{qr} \right] \\ v_{x1s} = r_s i_{x1s} + \frac{d}{dt} l_{fs} i_{x1s} \\ v_{y1s} = r_s i_{y1s} + \frac{d}{dt} l_{fs} i_{x1s} \\ v_{x2s} = r_s i_{x2s} + \frac{d}{dt} l_{fs} i_{x2s} \\ v_{y2s} = r_s i_{y2s} + \frac{d}{dt} l_{fs} i_{y2s} \\ 0 = r_r i_{dr} + \frac{d}{dt} \left[(l_{fr} + L_m) i_{dr} + L_m i_{ds} \right] - \omega_r \left[(l_{fr} + L_m) i_{qr} + L_m i_{qs} \right] \\ 0 = r_r i_{dr} + \frac{d}{dt} \left[(l_{fr} + L_m) i_{qr} + L_m i_{qs} \right] + \omega_r \left[(l_{fr} + L_m) i_{dr} + L_m i_{ds} \right] \end{cases}$$

The electromagnetic torque developed by the motor expressed in terms of stator and rotor currents is given by:

$$\Gamma_{em} = \frac{1}{2} \begin{pmatrix} \begin{bmatrix} i_{ds} \\ i_{qs} \\ i_{dr} \\ i_{ar} \end{bmatrix} \end{pmatrix}^{t} \begin{pmatrix} \frac{\partial}{\partial \theta} \begin{bmatrix} [L_{s}] & [M_{sr}] \\ [M_{rs}] & [L_{r}] \end{bmatrix} \end{pmatrix} \begin{pmatrix} \begin{bmatrix} i_{ds} \\ i_{qs} \\ i_{dr} \\ i_{ar} \end{bmatrix} \end{pmatrix}$$
(6)

After calculation, the following equation is obtained:

$$\Gamma_{em} = PL_m(i_{dr}i_{qs} - i_{qr}i_{ds}) \tag{7}$$

with: i_{ds} , i_{qs} , i_{x1s} , i_{y2s} , i_{x2s} , i_{y2s} , i_{dr} , i_{qr} are respectively the stator and rotor currents components, v_{ds} , v_{qs} , v_{x1s} , v_{y1s} , v_{x2s} , v_{y2s} , v_{dr} , v_{qr} are stator and rotor voltages components, ψ_{ds} , ψ_{qs} , ψ_{x1s} , ψ_{y1s} , ψ_{x2s} , ψ_{y2s} , ψ_{dr} , ψ_{qr} , are respectively the stator and rotor fluxes components, and the parameters of each seven phase induction motor are given in Table 1.

PEMFC dynamics model

There are several approaches to modeling a fuel cell, such as the theoretical approaches, the semi-empirical approach and the energy approach. The choice of an approach or other is closely related to the desired level of detail of the model, i.e. its complexity. The level of complexity determines, on the one hand, the modeled zone of the fuel cell system (it may be part or all of a cell, the stack and its auxiliary systems), and the fineness with which the modeled elements are described [14].

The energy approach is original both from the point of view of the community of Electrochemistry and that of Electrical

Table 1 - Parameters of seven phase induction machine.

Parameters	Symbol	Values	Units
Nominal Power	P_n	18.2	kW
Nominal Frequency	f	50	Hz
Stator Resistance	r_s	0.88	Ω
Rotor Resistance	r_r	0.55	Ω
Stator Leakage Inductance	l _{fs}	0.0036	Н
Rotor Leakage Inductance	l_{fr}	0.0036	Н
Mutual inductance	L_m	0.03816	Н
Inertia Moment	J	0.6	N.m.s/rd
Pole number	р	4	

Engineering. It is a question of modeling all the energy flows (electric, thermal, fluidic) within an electrochemical component.

In this work, the PEMFC is the main energy source for the vehicle. Its cell voltage and its total power are defined by the following equations [14,15]:

$$\begin{cases} V_{fc} = N_0 V_{fc,cell} \\ V_{fc,cell} = E + U_{act} + U_{ohm} \\ U_{ohm} = -R_{fc} i_{fc} \\ U_{act} = -\frac{B}{N_0} ln(Ci_{fc}) \end{cases} \tag{8}$$

The expression of the Nernst equation according to JC Pamphlet is given by Ref. [16]:

$$E_{\text{Nernst}} = E_0 + \frac{RT_{fc}}{2F} \ln \left(\frac{P_{H_2} \sqrt{P_{O2}}}{P_{H_2O}} \right)$$
 (9)

The FC should be able to provide the power demand of the vehicle P_{Load} by taking into account the FC efficiency η_{fc} .

The molar flow of a gas (hydrogen or oxygen) through a certain valve is proportional to its partial pressure. This relationship can be expressed as [16]:

$$\begin{cases} \frac{q_{H_2}}{P_{H_2}} = K_{H_2} \\ \frac{q_{O_2}}{P_{O_2}} = K_{O_2} \\ \frac{q_{H_2O}}{P_{H_2O}} = K_{H_2O} \end{cases}$$
 (10)

where K_{H_2} and K_{O_2} are the hydrogen and oxygen valve constants respectively.

Using the ideal gas formula and writing the molar flows as q^{in} , q^{out} and q^r , the partial pressures derivation is expressed as:

$$\begin{cases} \frac{d}{dt} P_{H_2} = \frac{RT_{fc}}{V_{an}} \left(q_{H_2}^{in} - q_{H_2}^{out} - q_{H_2}^r \right) \\ \frac{d}{dt} P_{O_2} = \frac{RT_{fc}}{V_{an}} \left(q_{O_2}^{in} - q_{O_2}^{out} - q_{O_2}^r \right) \\ \frac{d}{dt} P_{H_2O} = \frac{RT_{fc}}{V_{an}} \left(- q_{H_2O}^{out} + q_{H_2O}^r \right) \end{cases}$$
(11)

As the electromechanical fundamentals are taken in consideration, the molar flows of the both gas can be written as:

$$\begin{cases} q_{H_2}^r = \frac{N_0}{2F} I_{fc} = 2K_r I_{fc} \\ q_{O_2}^r = \frac{N_0}{4F} I_{fc} = K_r I_{fc} \\ q_{H_2O}^r = \frac{N_0}{2F} I_{fc} = 2K_r I_{fc} \end{cases}$$
(12)

where:

$$\begin{cases} \frac{d}{dt} P_{H_2} = \frac{RT_{fc}}{V_{an}} \left(q_{H_2}^{in} - K_{H_2} P_{H_2} - 2K_r I_{fc} \right) \\ \frac{d}{dt} P_{O_2} = \frac{RT_{fc}}{V_{an}} \left(q_{O_2}^{in} - K_{O_2} P_{O_2} - K_r I_{fc} \right) \\ \frac{d}{dt} P_{H_2O} = \frac{RT_{fc}}{V_{an}} \left(K_{H_2O} P_{H_2O} + 2K_r I_{fc} \right) \end{cases}$$
(13)

Assuming that the initial conditions of the hydrogen and oxygen partial pressures are null, the Laplace transforms of (13) as:

$$\tau_{H_2} = \frac{V_{\text{an}}}{K_{H_2} R \; T_{fc}}; \quad \tau_{O_2} = \frac{V_{\text{an}}}{K_{O_2} R \; T_{fc}} \quad \text{and} \quad \tau_{H_2O} = \frac{V_{\text{an}}}{K_{H_2O} R \; T_{fc}}$$

UC system modelina

The choice of the auxiliary source is carried on the UC because of its high power density and its charge and discharge time, comparing it to the battery [15,17]. In addition, it is the most robust and has a low maintenance cost. By using the simple mathematical model (see Fig. 2), the UC model is expressed as following:

$$\left\{ \begin{array}{l} V_{cell} = r_s i_{cell} + \frac{1}{C_{cell}} \int \left(i_{cell} - \frac{V_{cell}}{r_p}\right) \\ V_{UC} = n_{UC} V_{cell} \\ SOC(t) = \frac{V_{UC}^2(t)}{V_{UC,max}^2} \end{array} \right\} \tag{14}$$

Dynamics model of vehicle

Energy and power are imposed by the dynamics of the vehicle under different conditions (driving cycle) which defines the path to be traveled. The power P_{ν} is equal to the power present at the level of the wheels expressed by:

$$P_{v} = P_{Load} = \Gamma_{T} \cdot \Omega_{wheel} \tag{15}$$

where the total torque Γ_T and the speed of rotation of the

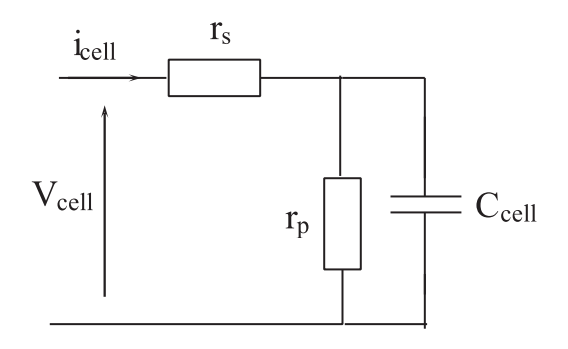


Fig. 2 - Equivalent circuit of UC bank.

wheel Ω_{wheel} are calculated directly from the traction force F_T and the speed V_{VEH} of the VE:

$$\begin{cases}
\Gamma_{\rm T} = F_{\rm T} \cdot \mathbf{r} \\
\Omega_{\rm wheel} = \frac{V_{\rm VEH}}{\mathbf{r}}
\end{cases}$$
(16)

with r the radius of the wheel.

The tensile force required to move the vehicle is given by the sum of the forces resisting the advancement added to the acceleration force F_{acc} [18]. As shown in Fig. 3, the rolling resistant forces detailed by system (17) are:

- The aerodynamic force Faero;
- The force F_{wheel} due to the contact of the wheels on the roadway;
- The gravitational force F_{gx} due to the slope α .

$$\begin{cases}
F_{aero} = 0.5 \cdot \rho \cdot A_{f} \cdot C_{x} \cdot V_{VEH}^{2} \\
F_{wheel} = M_{VE} \cdot g \cdot C_{r} \cdot V_{VEH} \cos(\alpha) \\
F_{qx} = M_{VE} \cdot g \cdot \sin(\alpha)
\end{cases}$$
(17)

These forces are therefore expressed as a function of the mass of the vehicle (Table 2). Thus, the power of the vehicle required for a mission can be given again by:

$$P_{Load} = \left(M_{VE} \cdot \frac{dV_{VEH}}{dt} + F_{aero} + F_{wheel} + F_{gx}\right) \cdot V_{VEH} \tag{18} \label{eq:pload}$$

Electrical differential

In order to test the performance of the electric differential used in an electric vehicle, there are two interesting situations:

- The linear regime, where both engines operate at the same speed;
- The rotating speed, where each motor runs at different speeds (Fig. 4).

The speed of rotation for each motor depends on the type of conduct and the plan chosen. For the direct line speed, the speeds of rotation for each motor become:

$$V_{rd} = V_{rg} = \frac{V_{VEH}}{r} \tag{19}$$

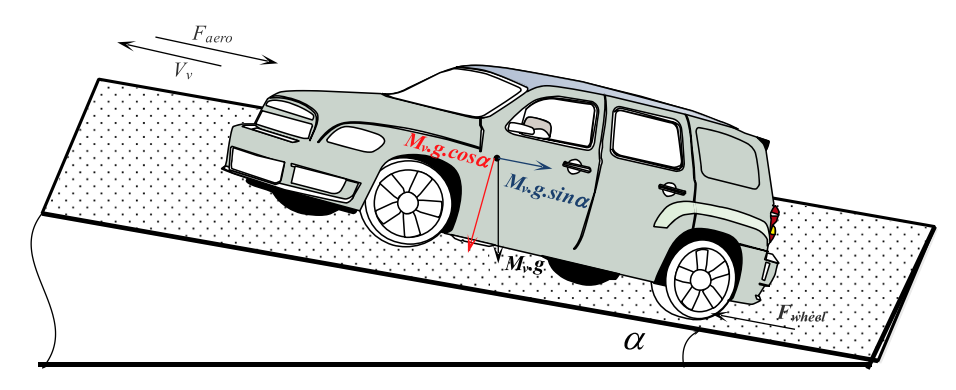


Fig. 3 – Dynamics of the vehicle.

Table 2 — Parameters of hybrid vehicle.					
Parameters	Symbol	Values			
Air Density	ρ	1.22 kg/m ³			
Frontal Surface Area of the Vehicle	A_f	1 m ²			
Aerodynamic Drag Coefficient	C_{x}	0.32			
Vehicle Total Mass	M_{VE}	1200 kg			
Tire Radius	r	0.33 m			

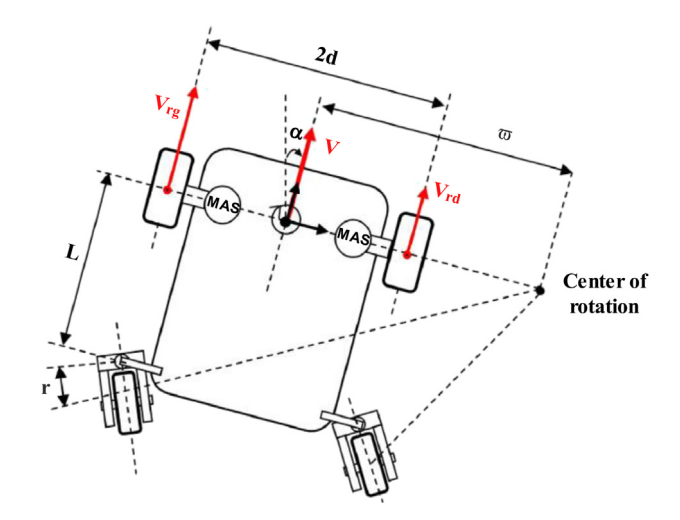


Fig. 4 - Electric differential.

For the rotational speed, the angular velocities for each motor are different and expressed as follows [19,20]:

$$V_{rd} = \frac{2V_{VEH}}{\left[1 + \frac{\omega + \frac{2r}{2r}}{\omega - \frac{2r}{2r}}\right]r} = \frac{V_{VEH}}{r} + \Delta\omega$$
 (20)

$$\Delta \omega = d \frac{V_{VEH}}{\varpi r} \tag{21}$$

Avec:

 $\Delta\omega$: Imposed during cornering

Control system

Direct field oriented control of seven phase induction motor

This section is devoted to the development of the seven phase induction machine control, the decoupling between rotor flux and electromagnetic torque is very important. This vector control is not very different from the conventional vector control; the aim is always to assimilate the behavior of induction machine to that to the DC machine separately excited by decoupling control of torque of the flux. But the difference lies in the minimization of non-sequential components [9]. This section allowed us to identify a new problem related to this type of machine. Several authors [5,21,22] have neglected these non-sequential components, making the controls developed over the incomplete work, the minimization of copper losses are very important for improving the efficiency of the machine. Otherwise the power segmentation loses its

importance; the control without consideration of its parasitic currents is incomplete. These components have an uncertain behavior, frequencies and scales variants making their filtering in transient regime via conventional filter (low pass, high pass, ... etc.) difficult and sometimes impossible. The solution that the author proposed in Ref. [10], consists of placed impedance filters in series with the stator windings of the machine with high harmonics and low fundamental frequencies. This solution is not only cumbersome but also very limited as it is valid in the steady state. In this section filtering of these streams and minimization via fuzzy logic is presented.

To simplify the model given by Eq. (5), the stator currents (i_{ds}, i_{qs}) , the rotor flux (ψ_{ds}, ψ_{qs}) , and the mechanical speed (Ω) , are considered as state variables. The orientation control by the rotor flux is to provide a decoupling between the magnitudes of the generating electromagnetic torque and rotor flux [6]. This can be done if the rotor flux coincides with the d-axis of the reference related to the rotating field. Thus, by acting on the variables i_{ds} , i_{qs} , quantities Γ_{em} and ψ_r are controlled separately; this means, align the rotor flux vector on the d-axis: $\psi_{dr} = \psi_r$ and $\psi_{qr} = 0$. The non-sequential components are not affected by the necessary processing for the orientation of the rotor field. By using this concept, the mathematical models of the seven phase induction machine become:

$$\begin{cases} \sigma L_{s} \frac{d}{dt} i_{ds} = -\left(r_{s} + \frac{L_{m}^{2}}{L_{r}^{2}} r_{r}\right) i_{ds} + \sigma L_{s} \omega_{s} i_{qs} + \frac{L_{m}}{T_{r} L_{r}} \psi_{dr} + \frac{L_{m}}{L_{r}} \omega_{r} \psi_{qr} + \upsilon_{ds} \\ \sigma L_{s} \frac{d}{dt} i_{qs} = -\left(r_{s} + \frac{L_{m}^{2}}{L_{r}^{2}} r_{r}\right) i_{qs} - \sigma L_{s} \omega_{s} i_{ds} + \frac{L_{m}}{T_{r} L_{r}} \psi_{qr} - \frac{L_{m}}{L_{r}} \omega_{r} \psi_{dr} + \upsilon_{qs} \\ \frac{d}{dt} \psi_{dr} = \frac{L_{m}}{T_{r}} i_{ds} + \omega \psi_{qr} - \frac{1}{T_{r}} \psi_{dr} \\ \frac{d}{dt} \psi_{qr} = \frac{L_{m}}{T_{r}} i_{qs} - \omega \psi_{dr} - \frac{1}{T_{r}} \psi_{qr} \\ \Gamma_{em} = P \frac{L_{m}}{L_{r}} \left(\psi_{dr} i_{qs} - \psi_{qr} i_{ds} \right) \\ J \frac{d}{dt} \Omega_{r} = \Gamma_{em} - \Gamma_{r} - f \Omega_{r} \end{cases}$$

$$(22)$$

with: J and Ω are the inertia and speed of the machine respectively.

Which induces:

$$\begin{cases} \psi_r^* + T_r \frac{d}{dt} \psi_r^* = L_m i_{ds} \\ \Gamma_{em}^* = P \frac{L_m}{L_r} i_{qs} \psi_r^* \\ \omega_s^* - \omega_r = \frac{L_m i_{qs}}{T_r \psi_r^*} \\ \theta_s^* = \int \omega_s^* dt \end{cases} \Rightarrow \begin{cases} \psi_r^* = \frac{L_m}{1 + s T_r} i_{ds} \\ \Gamma_{em}^* = P \frac{L_m}{L_r} i_{qs} \psi_r^* \\ \theta_s^* = \int \left(P\Omega + \frac{L_m i_{qs}}{T_r \psi_r^*} \right) dt \end{cases}$$

We can notice that only the direct component i_{ds} , determines the amplitude of the rotor flux, while the torque depends only on the quadrate component i_{qs} if the rotor flux is kept constant. Thus, the decomposition is carried out of the stator current into two terms corresponding to the flux and torque. For this, we obtain a similar structure to that of a DC

machine. The new DRFOC diagram of seven-phase induction motor is presented in Fig. 5. For the minimization of the non-sequential components, the fuzzy logic controller is used. About the definition of membership function, these controllers adheres to inputs (e(k),de(k)), and single output S(k). The membership functions illustrate the degrees to which specify attention belongs to the fuzzy set [23]. The membership degrees of account indicate each degree can be accounted quantitatively accomplished a set of formulae of membership functions. To convert these variables in the linguistic variables, the following seven membership functions are chosen for the input and output: NB: Negative Big, NM: Negative

Table 3 — Rules base for fuzzy logic control.							
E dE	NL	NM	NS	Z	PS	PM	PL
NL	NL	NL	NM	NM	NS	NS	Z
NM	NL	NM	NM	NS	NS	Z	PS
NS	NM	NM	NS	NS	Z	PS	PS
Z	NM	NS	NS	Z	PS	PS	PM
PS	NS	NS	Z	PS	PS	PM	PM
PM	NS	Z	PS	PS	PM	PM	PL
PL	Z	PS	PS	PM	PM	PL	PL

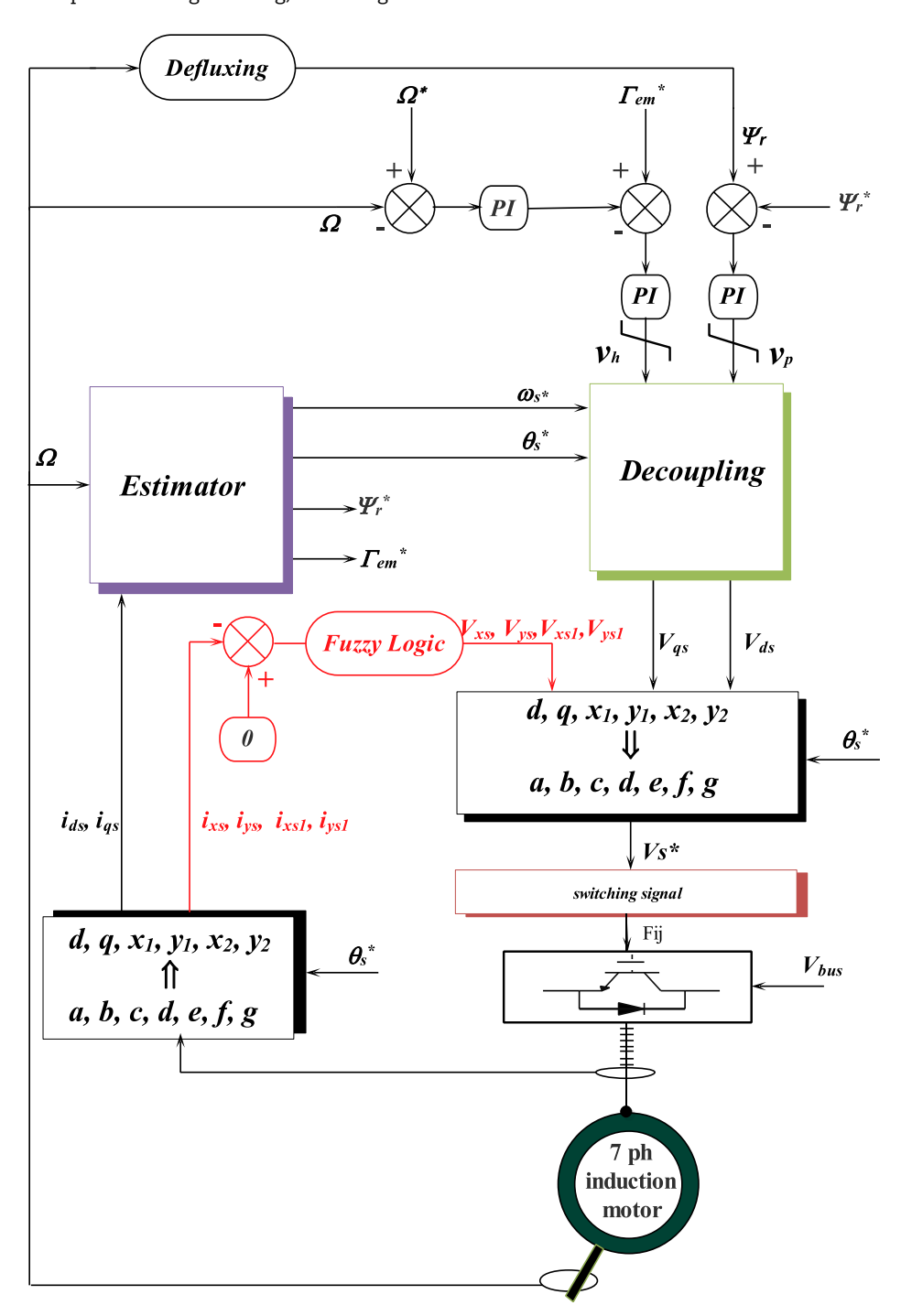


Fig. 5 – DRFOC of Seven Phase induction motor.

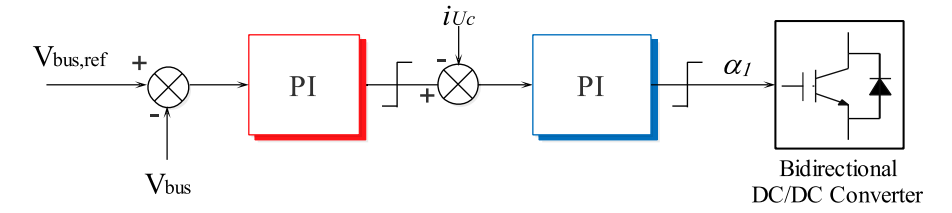


Fig. 6 – DC bus voltage regulation and the UC converter control.

Table 4 — Parameters of UC model.				
Parameters	Symbol	Values	Units	
Nominal Voltage	V _{cell}	16.2	V	
Electrical Capacitor	C_{UC}	500	F	
Electrical Series Resistance	r_s	2.4	$m\Omega$	
Maximum Power	$P_{UC,max}$	38	kW	

Medium, NS: Negative small, ZE: Zero Equal, PS: Positive Small, PM: Positive Medium, PB: Positive Big. Constriction domain variable Z provides better system responsiveness when the static error is small. The input of this controller variables are error "e" and the derivative of the error "de". It is possible to choose a large number of inferences tables. The one presented in Table 3 is chosen. All parameters of this regulator have been fit using several simulations. Algorithmic cost is very high, but the rejection of disturbances is effective. In addition, this controller can do without compensation algorithms. Further, to decrease the torque ripples the three levels NPC inverter is used.

DC bus voltage regulation and UC converter control

The regulation of the DC bus voltage is showed in Fig. 6 and Table 4 give the different parameter of the UC. The UC power is controlled indirectly by the regulation of the DC bus voltage. If there is power demand by the vehicle, the DC bus voltage decrease, an error voltage with its reference will be generated and give the rapport cyclic α_1 to control the IGBTs of the converter. The UC gives the necessary power to keep up the DC bus voltage. If the DC bus voltage is increased, the UC absorbs the excess power and the voltage decrease to its reference. This method allows to control also the UC current and make it a limitation to $i_{UC, max}$ and $i_{UC, min}$.

Fc converters control

The method of control power for the FC system is presented in Fig. 7 and the FC parameter are given in Table 5. The rapport

Table 5 $-$ Parameters of the FC model.					
Parameters	Symbol	Values	Units		
Activation Over Voltage Constants	В	0.0477	V		
Hydrogen Valve Constant	K_{H_2}	$4.22 \cdot 10^{-5}$	k.mol.atm/s		
Oxygen Valve Constant	K_{O_2}	$2.11 \cdot 10^{-5}$	k.mol.atm/s		
Oxygen Valve Constant	K_{H_2O}	$7.716\!\cdot\! 10^{-6}$	k.mol.atm/s		
Water Valve Molar Constant	$ au_{ m H_2O}$	18.418	S		
Number of Cells in Series in the	N_0	375			
Stack					
Fuel Cell Internal Resistance	R_{fc}	0.003	Ω		
Absolute Temperature	T_{FC}	343	K		
Universal Gas Constant	R	8314.47	J/(kmol K)		
Volume of Anode	V_{an}	150	m^3		
Nominal Power	$P_{nominal}$	30	kW		

cyclic α_2 is generated by the error between $i_{FC, ref}$ and i_{FC} . If the stat of charge of the UC system is low, the control allows charging the UC with the high efficiency for the FC and the UC system as follow:

Simulation results and interpretation

This part describes the simulation environment used to test and analyze the control algorithm developed during this work. The simulation context should incorporate models appropriate to the various components of the powertrain, the electrical machine and the power source. A three-stage velocity profile in Fig. 8 is used, the first between [0.2] s with a speed of each motor which is equal to $100 \, rd/s$, which is almost $120 \, km/h$ during this acceleration, each motor develops the same electromagnetic torque as illustrated in Fig. 9. In the second level we distinguish two speeds, the first is $60 \, rd/s$ which is around $71 \, km/h$, the rules $(\Delta \omega)$ is applied when passing in a turn. The latter imposes a difference between the speeds of the two motors, this difference also appears in electromagnetic torque, motor current see Fig. 10 and quadratic current see Fig. 11. In the third stage, for an average

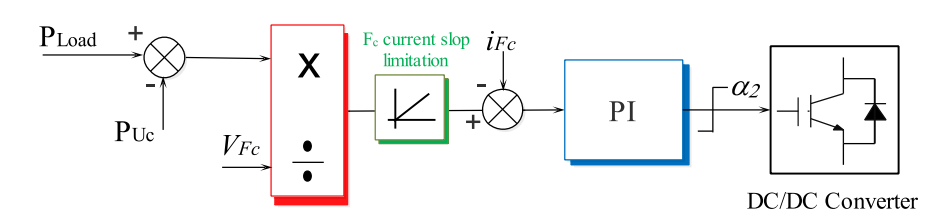


Fig. 7 - FC converter control.

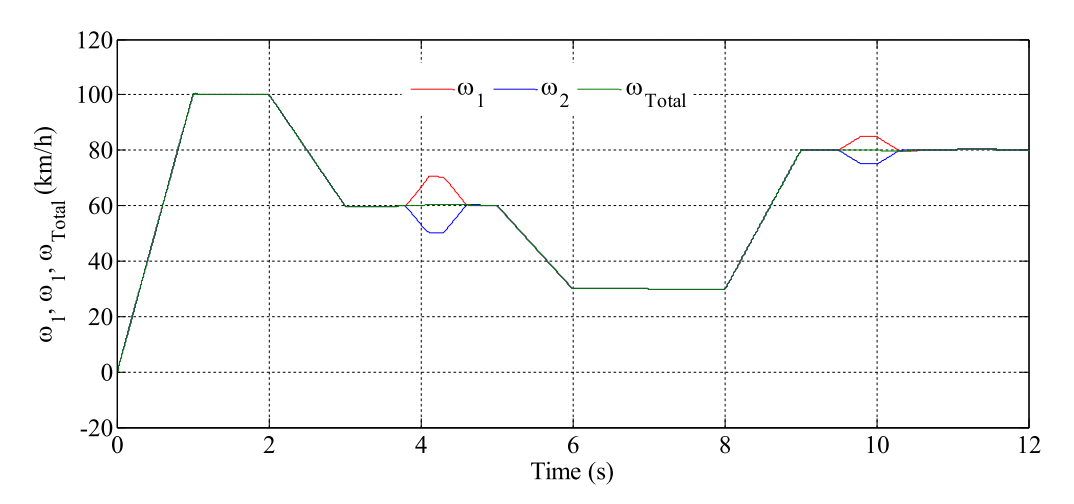


Fig. 8 - Mechanical speed.

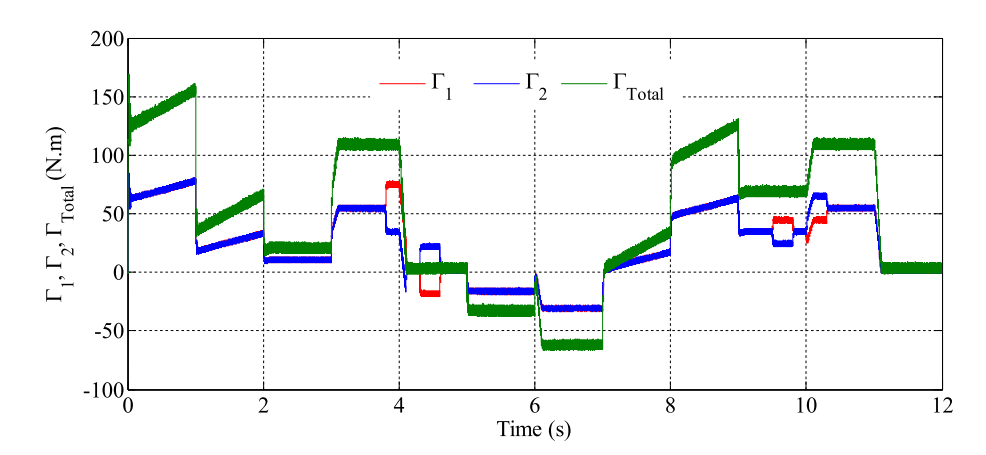


Fig. 9 - Electromagnetic torque.

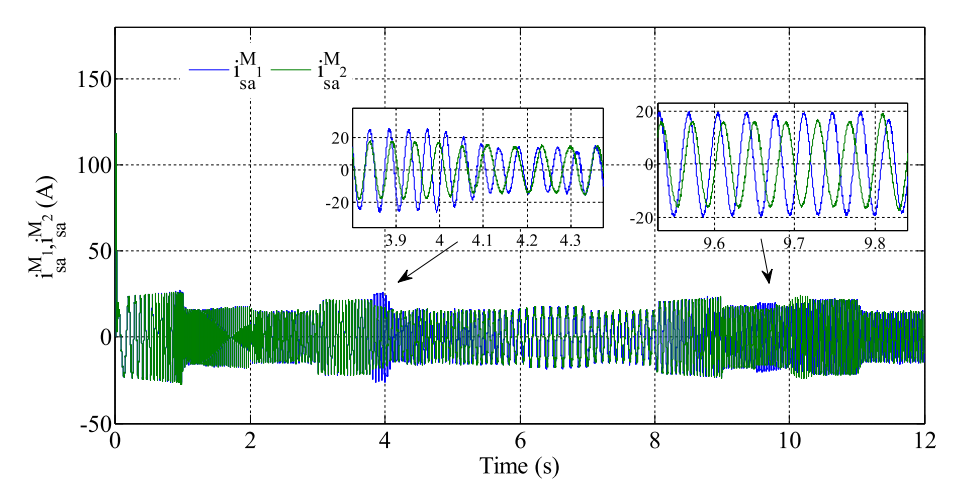


Fig. 10 - First phase current.

speed which is equal to 95 km/h, another setpoint ($\Delta\omega$) lower than the first one has been applied, which in this case also imposes a difference between the different mechanical and electrical variables of the two Engines. This difference does not affect the current of the direct axis, which is shown on the see Fig. 12. The currents of the two secondary part of the first

motor and the projection of the two current vectors in their own planes, respectively. Their amplitudes are almost nil see Fig. 13.

Fig. 14 shows the three powers of the system, namely the power demanded by the vehicle and the two powers delivered by the two on-board sources. The UC responds not only to the

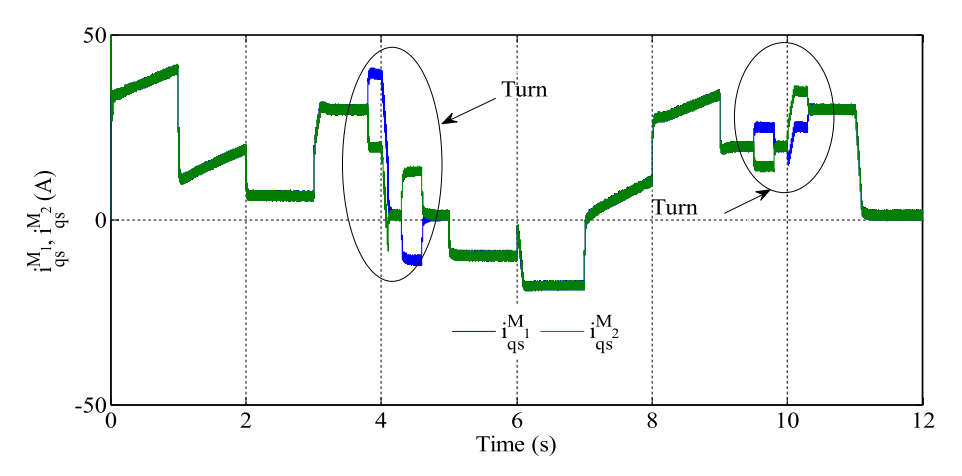


Fig. 11 - Quadratic current.

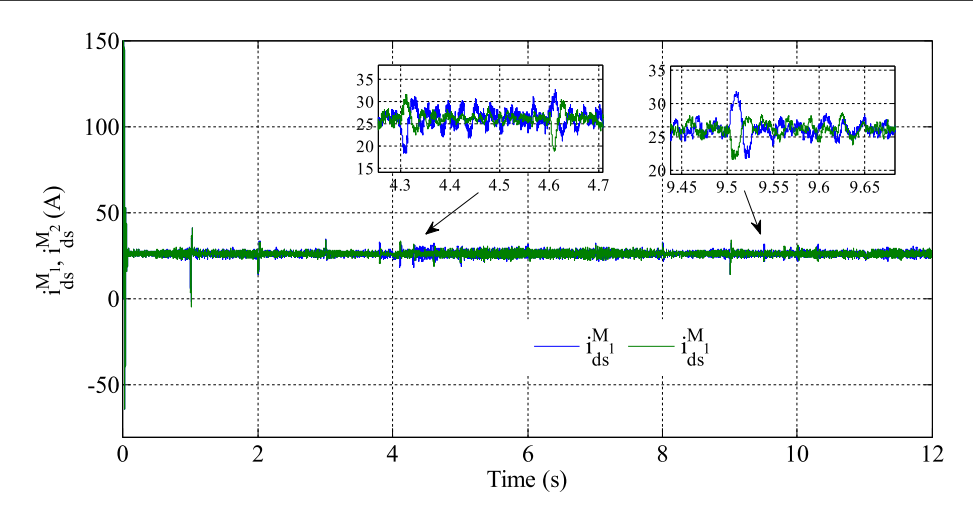


Fig. 12 - Direct current.

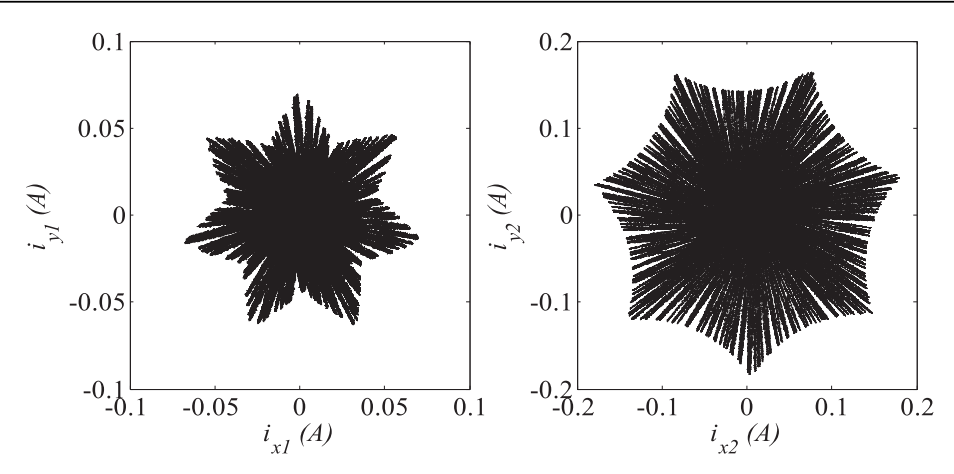


Fig. 13 – Currents of the two sub-machines in the planes (x1, y1) and (x2, y2).

high power demand, but also dampens the perturbation generated by the hash frequency of the two converters see Fig. 15. Moreover, the good quality of the power demanded by the vehicle, which is due to the decrease in the amplitude of the non-sequential currents, leads to an extension of the

lifetime of the fuel cell. Fig. 16 shows the variation of SoC, according to the powers supplied to the load. The power of the load is obtained by the sum of the powers of the FC, SC. During the energy recovery phase, the power supplied by the load is recovered by SC as shown in Figs. 14–16.

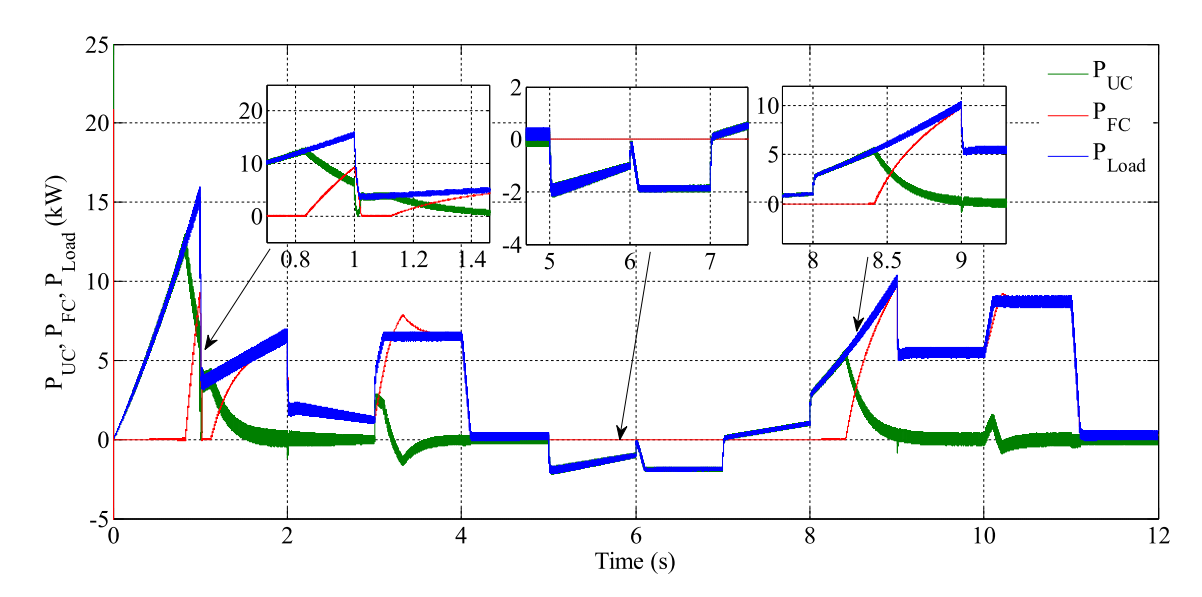


Fig. 14 - System's power.

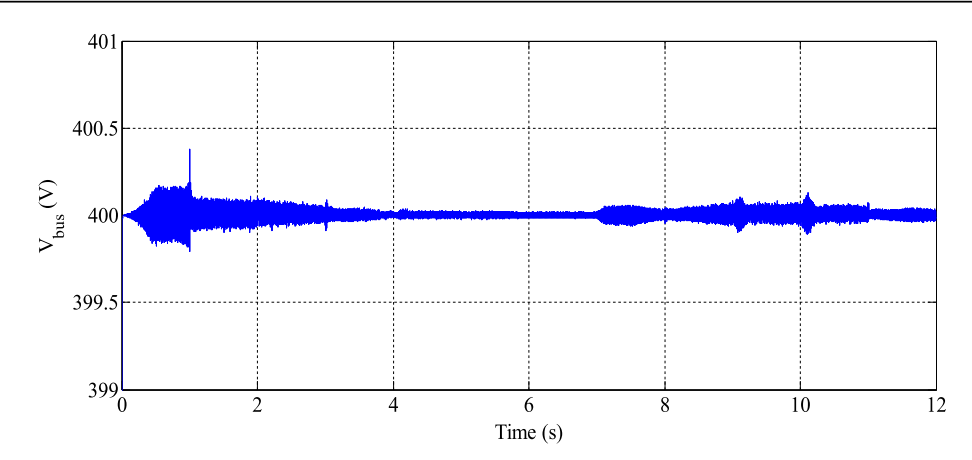


Fig. 15 - DC voltage.

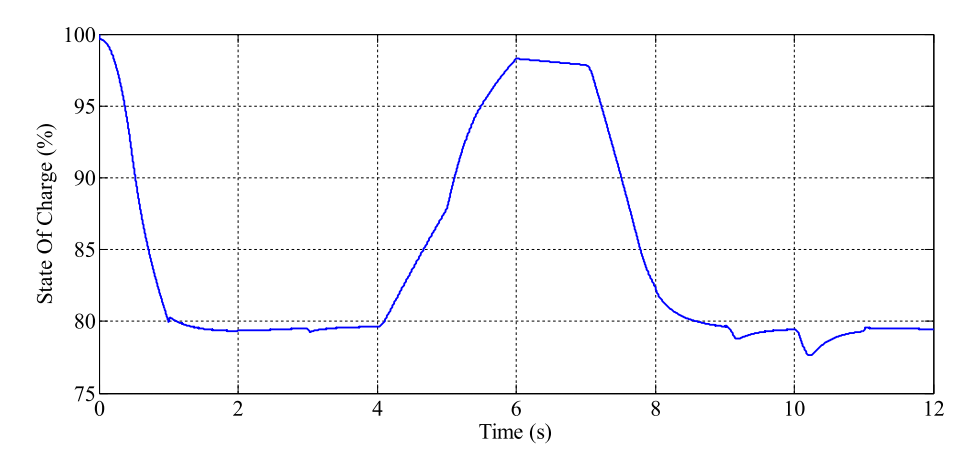


Fig. 16 - UC's state of charge.

Therefore, in order to avoid too rapid changes to the FC, the total energy is supplied by the SC secondary source in each requested power peak.

The FC is also reacting in order to keep the SC state of charge at its benchmark of 80%, but in a long way, which helps prolong the life of FC.

The main objective of this hybridization is to ensure a fuel cell dynamics limited mainly by its response time, to control the state of charge of the storage device (SC) and to bring or absorb the power required by the load. By improving the quality of the power required and filtering the noise caused by the static converters, a discrete system and a better comfort are obtained with this application. This is very favorable for applications intended for an increasingly demanding audience.

Conclusion

In this paper, hybridization of the two FC/SC sources is studied. This architecture is equipped with a fuel cell connected to the DC bus via a lifting chopper. Also, the need to use an energy storage system hybridized with the cap, in order to have a system allowing optimal operation. The storage means is connected to the DC bus through DC/DC converters. These converters have made it possible to regulate the DC bus voltage and to manage the transfer of the power to the load.

Further, the vector control of seven phase induction machine with fuzzy controllers is used in favor of the HEV. The modeling of seven-phase induction machine shows that is composed by three parts. Firstly, components are the principal part that produces electromagnetic torque. On the other hand, parts do not contribute to the torque production, but this is a real problem of the electrical and mechanical power's quality, the degradation of this last are caused by voltage harmonics. One inconvenient of using the polyphase induction machine is non-sequential currents overlapping the main currents of the machine. The behavior of these currents is unknown, hence the need to use fuzzy logic to minimize these parasitic currents and minimizing losses and leaks in the machine.

This improvement in the quality of energy affects the lifetime of the on-board source. Moreover, the role of the UC's and very favorable to saving of the fuel cell and the extension of its lifetime.

REFERENCES

- [1] Leonard W. Control of electrical drives. Editions Springer; 1996.
- [2] Aissou R, Rekioua T, Rekioua D, Tounzi A. Robust nonlinear predictive control of permanent magnet synchronous generator turbine using Dspace hardware. Int J Hydrogen Energy 7 December 2016;41(45):21047–56.
- [3] Soufi Y, Kahla S, Bechouat M. Particle swarm optimization based sliding mode control of variable speed wind energy conversion system. Int J Hydrogen Energy 7 December 2016;41(45):20956–63.
- [4] Tazerart F, Mokrani Z, Rekioua D, Rekioua T. Direct torque control implementation with losses minimization of induction motor for electric vehicle applications with high operating life of the battery. Int J Hydrogen Energy 19 October 2015;40(39):13827–38.
- [5] Levi E, Bojoi V, Profumo F, Toliyat HA, Williamson S. Multiphase induction motor drives — a technology status review. IET Electr Power Appl 2007;1(4):489—516.

- [6] Klingshirn EA. High phase order induction motors-Part-I-Description and theoretical considerations. IEEE Trans PAS 1983;102(1):47-53.
- [7] Vas P. Vector control of AC machines. Oxford Science Publication; 1994.
- [8] Dieng A, Benkhoris MF, Mboup AB, Aït-Ahmed M, Le Claire JC. Behavior analysis of Five phase permanent magnet synchronous motor-voltage source inverter drive based on Fortescue transformation. Revue Roumaine Sci Serie Electrotechnique et Energ 2016;61(2):116–20. Bucarest.
- [9] Iffouzar K, Benkhoris MF, Ghedamsi K, Aouzellag D. Behavior analysis of dual stars induction motor supplied by PWM multilevel inverters. Revue Roumaine Sci Serie Electrotechnique et Energ 2016;61(2):137–41. Bucarest.
- [10] Eugene A. Harmonic filters for six-phase and other multiphase motors on voltage source inverters. IEEE Trans Indust Appl 1985;IA-2I:588–94.
- [11] Azib A, Ziane D, Rekioua T. Ensure continuity of operation of an electric vehicle under fault condition in converter. Int J Hydrogen Energy 8 June 2016;41(21):9066–74.
- [12] Berudez M, Gonzalez-Prieto I, Barrero F, Guzman H, Duran MJ, Kestelyn X. Open-phase fault-tolerant direct torque control technique for five-phase induction motor drives. IEEE Trans Indust Electron Feb 2017;64(2):902—11.
- [13] I. Gonzalez-Prieto, M.J. Duran, F.J. Barrero. Fault-tolerant control of six-phase induction motor drives with variable current injection. IEEE Trans Power Electron 99:1.
- [14] Zheng CH, Oh CE, Park YI, Cha SW. Fuel economy evaluation of fuel cell hybrid vehicles based on equivalent fuel consumption. Int J Hydrogen Energy 2012;37:1790–6.
- [15] Garcia P, Torreglosa JP, Fernandez LM, Jurado F. Viability study of a FC-battery-SC tramway controlled by equivalent consumption minimization strategy. Int J Hydrogen Energy 2012;37:9368–82.
- [16] Paladini V, Donateo T, Arturo R, Laforgia D. Super-capacitors fuel-cell hybrid electric vehicle optimization and control strategy development. Energy Convers Manag 2007;48:3001—8.
- [17] Azib T, Bethoux O, Remy G, Marchand C. Saturation management of a controlled fuel cell/ultracapacitor hybrid vehicle. IEEE Trans Veh Technol 2011;60(9):4127–38.
- [18] Payman Alireza, Pierfederici Serge, Meibody Tabar Farid. Energy control of super capacitor/fuel cell hybrid power source. Energy Convers Manag 2008;49:1637–44.
- [19] Tabach B, Kheloui A, Henini N. An electric differential system for a two-wheel mobile platform using direct torque control with adaptive flux and speed observers. In: SPEEDAM, Italy; 2008.
- [20] Guazzelli RU, de Oliveira CMR, de Castro AG, Pereira WCA, de Aguiar ML. Electric vehicle hardware-in-the-loop simulation with differentiator optimised by genetic algorithm. In: 2016 12th IEEE International Conference on Industry Applications (INDUSCON), Curitiba, PR, Brazil; 2016. p. 1–8.
- [21] Iffouzar K, Taraft S, Aouzellag H, Ghedamsi K, Aouzellag D. DRFOC of polyphase induction motor based on fuzzy logic controller speed. In: 2015 4th International Conference on Electrical Engineering (ICEE); 13–15 Dec 2015. p. 1–7.
- [22] El-Barbary ZMS. Fuzzy logic based controller for five-phase induction motor drive system. Alexandria Eng J 2012;51:263—8.
- [23] Bouchiba B, Hazzab A, Glaoui H, Fellah MK, Bousserhane IK, Sicard P. Multiple-input multiple-output fuzzy sliding mode controller for multi-motors system. Rev Roum Sci Techn Électrotechn et Énerg 2012;57(2):202–11. Bucarest.